CFD Assessment of Forward Booster Separation Motor Ignition Overpressure on ET XT 718 Ice/Frost Ramp

Edward Tejnil[1]
Science & Technology Corp., NASA Ames Research Center, Moffett Field, CA, 94035

Stuart E. Rogers[2]
NASA Ames Research Center, Moffett Field, CA, 94035

Computational fluid dynamics assessment of the forward booster separation motor ignition over-pressure was performed on the space shuttle external tank X_T 718 ice/frost ramp using the flow solver OVERFLOW. The main objective of this study was the investigation of the over-pressure during solid rocket booster separation and its affect on the local pressure and air-load environments. Delta pressure and plume impingement were investigated as a possible contributing factor to the cause of the debris loss on shuttle missions STS-125 and STS-127. A simplified computational model of the Space Shuttle Launch Vehicle was developed consisting of just the external tank and the solid rocket boosters with separation motor nozzles and plumes. The simplified model was validated by comparison to full fidelity computational model of the Space Shuttle without the separation motors. Quasi steady-state plume solutions were used to calibrate the thrust of the separation motors. Time-accurate simulations of the firing of the booster-separation motors were performed. Parametric studies of the time-step size and the number of sub-iterations were used to find the best converged solution. The computed solutions were compared to previous OVERFLOW steady-state runs of the separation motors with reaction control system jets and to ground test data. The results indicated that delta pressure from the over-pressure was small and within design limits, and thus was unlikely to have contributed to the foam losses.

Nomenclature

A_t/A_i	=	nozzle throat to inlet area ratio
α	=	angle of attack
β	=	angle of side slip
ΔP	=	difference in pressure
ΔP_{max}	=	maximum difference in pressure
Δt	=	dimensional physical time step
ΔT	=	dimensional simulation time step
DT	=	computational time step
DTPHYS	=	physical time step
ϕ	=	circumferential coordinate of the tank
γ	=	specific heat ratio
ITIME	=	time-step scaling option
L_{ref}	=	reference length
MW	=	molecular weight
NITNWT	=	number of Newton/dual-time sub-iterations
P	=	pressure
P_0	=	nozzle inlet total pressure
P_∞	=	free-stream pressure

[1] Senior Research Scientist/Engineer.
[2] Aerospace Engineer, Associate Fellow AIAA.

P_{max} = maximum pressure
T_∞ = free-stream temperature
T_0 = nozzle inlet total temperature
$T(\Delta P_{max})$ = simulation time at ΔP_{max}
ρ_∞ = free-stream density
M_∞ = free-stream Mach number
Re = Reynolds number
T_∞ = free-stream temperature
$\bar{q}$ = free-stream dynamic pressure
U_{ref} = reference velocity

I. Introduction

During the ascent of the STS-127 mission of the Space Shuttle, a loss of foam from the Thermal Protection System (TPS) was observed from the liquid oxygen (LO2) portion of the External Tank (ET). The foam was lost from the Ice/Frost Ramp (IFR) located at station X_T 718 as seen in Fig. 1. The debris loss occurred immediately after Solid-Rocket Booster (SRB) separation at mission elapsed time (MET) of 126 seconds, when the vehicle was traveling at Mach 4.0. Figure 2 shows a photograph of the liberated foam in flight as seen from the LO2 feedline camera. Similar TPS losses occurred from the same IFR during the STS-125 mission. This paper is a result of the work conducted in support of the integrated in-flight anomaly (IIFA) STS-127-I-004 entitled "TPS Loss at LO2 IFR 718 Resolution." The exact cause of the foam loss was never officially determined. While the most likely cause of the foam loss was a pressurized void inside the foam, the current work was undertake to investigate the possible role of a pressure disturbance caused by the Booster Separation Motors (BSMs).

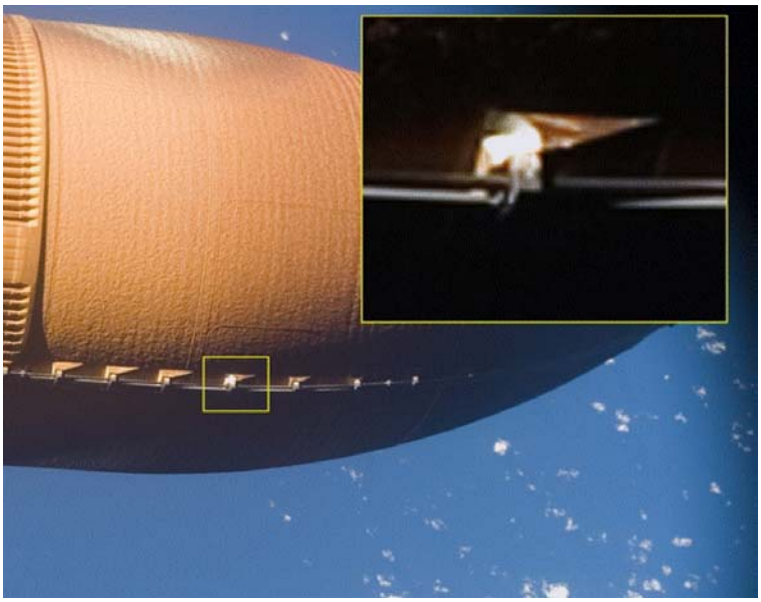

Figure 1. STS-127 TPS loss at LO2 IFR located at X_T=718 inches.

Figure 2. STS-127 TPS debris loss at MET=126 seconds (Ref. IIFA STS-127-I-004).

Figure 3. STS-117 SRB separation with BSM motors and RCS jets firing.

Approximately two minutes after the launch of the Space Shuttle, when the vehicle Mach number reaches 4.0, the SRB separation is initiated. The eight BSMs on each SRB fire for 1.02 seconds; four BSMs are located in the nose frustum, and four are located on the aft skirt.[1] The BSMs are fired to separate the SRBs from the Orbiter and the ET. In addition, the forward Reaction Control System (RCS) jets on the Orbiter are fired to prevent the BSM plume by-products from hitting the Orbiter windshield. Figure 3 shows a photograph of the SRB separation with both BSM motors and RCS jets firing. See Ref. 2-4 for descriptions of the SRB separation motors and their design.

The primary objective of this study was to perform a Computational Fluid Dynamics (CFD) assessment of the forward BSM ignition over-pressure (IOP) on the X_T 718 IFR, using a simplified model of the Space Shuttle Launch Vehicle (SSLV). The effects of the BSM IOP were investigated to determine if it caused significant changes in the aerodynamic environment local to the IFR.

Previous computational studies of IOP include work reported in Refs 5 and 6. Colombier and Pollet[5] performed some computational simulations of IOP. Houseman et al[6] report on extensive studies on the numerical simulation of IOP. Previous simulations of the SRB separation with the BSMs and the RCS jets firing were performed by Gea.[7] In this work the flow solver OVERFLOW[8,9] was used to compute steady-state solutions were at five different static positions during SRB separation. To model the high temperature nozzle flows and different plume species, the variable gamma option was utilized. Using this approach, the species continuity equations were solved to track the

mass fractions of the different gases. The resulting gamma of the gas mixture was computed by the mass-average of the individual gases. OVERFLOW simulations of the SSLV with real-gas solid rocket plume effects were presented in Ref. 10. The effects of the solid rocket exhaust plume on the Space Shuttle Orbiter flow field were examined in Ref. 11.

Two additional preceding works were performed by the Space Shuttle Program (SSP):

1) IFR 718 Aero Environments by R. Taylor, C. Ortiz of Boeing Co.
2) Forward Booster Separation Motor Ignition Overpressure on ET XT 718 Ice/Frost Ramp by L. Wong of Boeing Co.

In the first of these, the reported maximum delta pressure on the ET surface from OVERFLOW steady-state plume solutions of the BSMs and RCS jets firing was 0.2 psid. This is significantly lower than the design air-load from the SSP Operational Aerodynamics Databook (OADB) for the X_T 718 IFR, which is 8.4 psid. In the second of these, the results of a ground-firing test were presented, whose goal was to measure the IOP pulse from a single BSM motor at various distances in the far field. In the experiment, the measured projected 2-D single motor BSM IOP on the X_T 718 IFR was approximately 1.0 psid. To account for a cluster of 4 motors, an empirically-derived multiplying factor of 1.4 was applied, resulting in a projected 4 BSM cluster IOP of 1.4 psid.

In the current work, both steady-state plume and time-accurate BSM IOP simulations were performed with OVERFLOW. The full Reynolds-averaged Navier-Stokes (RANS) equations and the variable gamma option with two gas species were employed. The simplified geometry model was validated by comparison to results from a full fidelity CFD model of the SSLV without the separation motors firing. The thrust of the BSMs was calibrated using steady-state solutions, in which the nozzle boundary conditions were varied to match the known thrust of the motors. The plume impingement on the surface of the vehicle and corresponding change in surface pressure was determined from the steady-state solutions.

The time-accurate BSM IOP simulations were performed using Newton and dual-time sub-iterations in OVERFLOW to examine unsteady effects. Parametric studies using the computational time step (*DT*), the physical time step (*DTPHYS*), the time step scaling factor (*ITIME*) and the number of Newton/dual-time sub-iterations (*NITNWT*) were used to find the best converged solution. The effect of the over-pressure was examined with the maximum delta pressure bounds computed on a region where the IFR is located on the tank.

The following sections contain a description of the simplified SSLV model, the free-stream conditions, the computational approach, convergence of the CFD solution, results and data comparisons. The computer resource usage for the cases is also reported.

II. Simplified SSLV Model

The current computational study compares the three different geometries shown in Fig. 4, which are referred to as 1) ET-128 DCR, 2) ET+SRBs and 3) ET+SRB+BSMs cases respectively. In the first two geometries the BSM nozzles are not modeled, but they do include the sealed BSM canisters, which protrude from the SRB nose cones.

In order to minimize the computational cost, a simplified model of the SSLV is developed with only the geometry necessary to accurately predict the aerodynamics on the LO2 portion of the tank. Because the event occurred at supersonic free-stream Mach 4.0 conditions, the geometry downstream of the intertank could be neglected. The computational model consisting of a clean ET+SRBs geometry truncated at station X_T=1825 inches is shown in Fig. 5. The simplified geometry excluded the Shuttle Orbiter, LO2 feed-line, pressurization lines, IFRs and ET attach hardware.

In the current work, grid systems for the BSM nozzle geometries and corresponding plumes are introduced to capture the flow features of the motors firing. Each of the forward BSMs is represented with four nozzle+core and plume+core grids (see Fig. 6). The BSMs account for an additional 18 grid zones and approximately 30.6 million points.

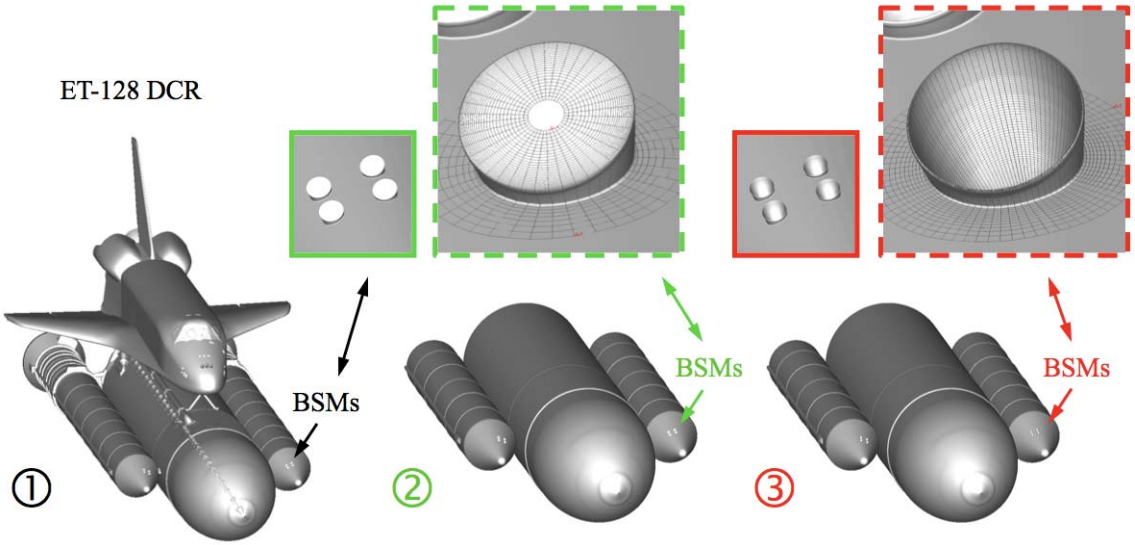

Figure 4. Comparison of the geometries: 1) ET-128 DCR, 2) ET+SRBs and 3) ET+SRBs+BSMs.

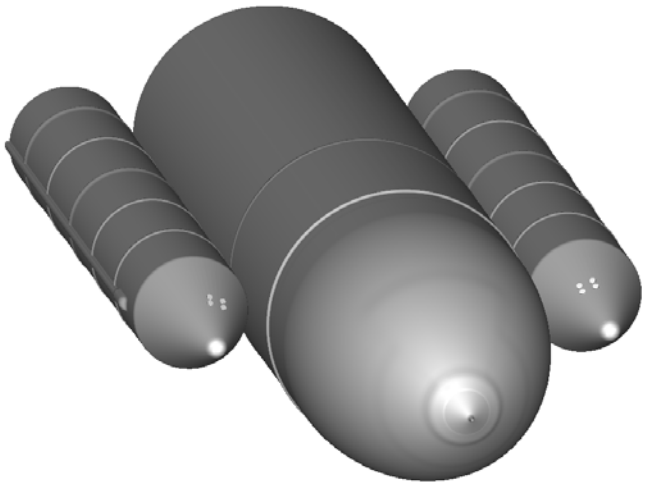

Figure 5. Expanded view of the ET+SRBs geometry which is truncated at X_T=1825 inches.

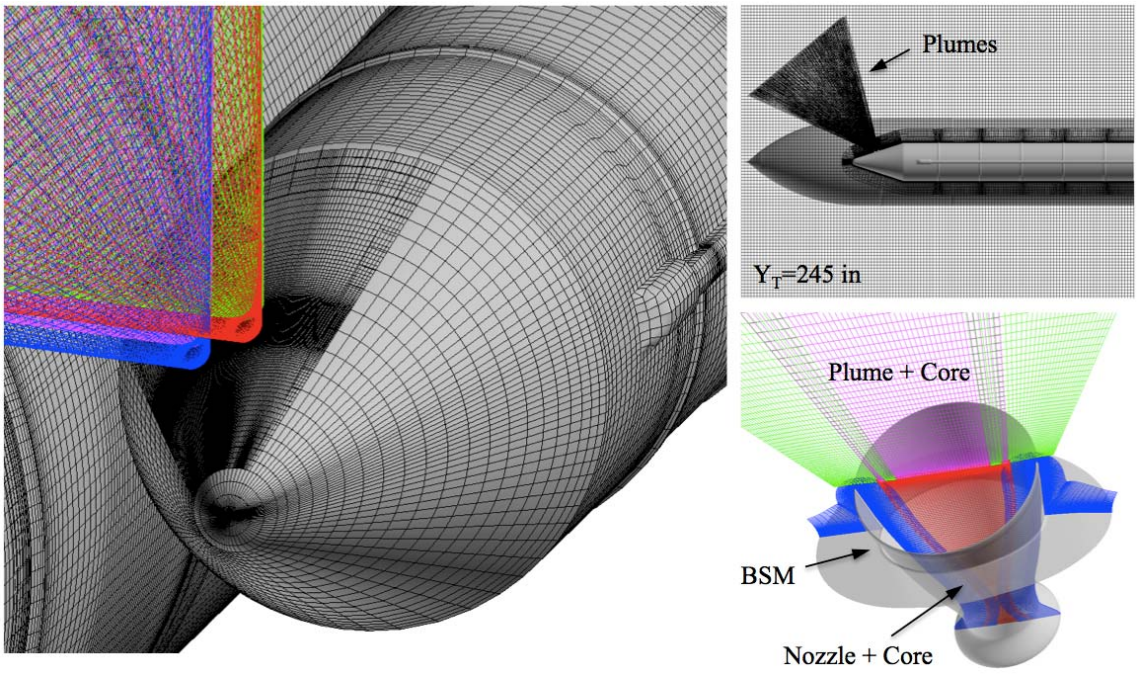

Figure 6. View of the BSM nozzles and plume grids in the ET+SRB+BSMs geometry.

All of the grids were generated with an automated grid-generation script specifically developed for this task. This process utilized the script library from the Chimera Grid Tools (CGT) software package.[12,13] The scripts generated the overset surface and volume grids using techniques detailed in Refs. 14 and 15. The scripts also generated all required input files for the flow solver and other utility codes. The overset domain connectivity was performed using the PEGASUS5[16] code, and the force and moment integration was performed using the MIXSUR and OVERINT[17] codes.

III. Free-stream Conditions and Grid Statistics

The free-stream flow conditions including Mach number (M_∞), angle of attack (α), angle of side slip (β), Reynolds number (Re), temperature (T_∞), dynamic pressure ($\bar{q}$), total number of grids (*ngrid*), total number of grid points (*npnts*) and version of OVERFLOW (*Solver*) are shown in Table 1. All of the overset grid generation was performed on the Columbia supercomputer using 32 CPUs. The ET-128 DCR geometry contained 629 zones, 97.4 million grid points and required approximately 2 hours to generate. The ET+SRBs and ET+SRBs+BSMs geometries contained 28 and 46 zones, 15.5 and 50.1 million points respectively and took approximately 10 minutes to generate. The vehicle reference length (*REFL*), reference area (*REFA*) and location of the moment center (*XMC*, *YMC*, *ZMC*) are listed below:

REFL = 1290.3 in
REFA = 387360.0 in^2
XMC = 976.0 in
YMC = 0.0 in
ZMC = 400.0 in

Table 1. Free-stream conditions and grid metrics for the ET-128 DCR, ET+SRBs and ET+SRBs+BSMs cases.

Case	M_∞	α deg	β deg	*Re* per inch	T_∞ $^\circ R$	$\bar{q}$ psf	*ngrid*	*npnts*	*Solver*
ET-128 DCR	3.909	4.300	0.081	3,221.9	481.4	28.6	629	97,445,962	2.1ae
ET+SRBs	3.909	4.300	0.081	3,221.9	481.4	28.6	28	19,462,471	2.1ae
ET+SRBs+BSMs	3.909	4.300	0.081	3,221.9	481.4	28.6	46	50,110,187	2.1ae

IV. Computational Approach

The computations were performed with the CFD flow solver OVERFLOW, version 2.1ae on NASA Ames Columbia[18,19] and Pleiades[20] supercomputers. OVERFLOW is a viscous compressible code developed by NASA, which solves the time-dependent RANS equations using structured overset[21] grids. To improve numerical accuracy, solution stability and robustness, a third-order spatial upwind convective flux scheme HLLC[22] in combination with an implicit unfactored SSOR[23] algorithm and scalar dissipation was employed. The HLLC Riemann algorithm can handle extremely large gradients in the flow and has been shown to produce good results for a wide range of Mach numbers. The SSOR algorithm eliminates the factorization error at the expense of more computational work and memory. The flow was assumed to be fully turbulent, with all viscous terms, including cross terms, turned on in the code. The one-equation Spalart-Allmaras (SA) turbulence model[24] was utilized. To model the BSM nozzle plumes with a supersonic incoming cross flow at Mach 4.0, the variable gamma option was employed with two gas species (Air, BSM gas).

The input files containing the power BCs for the BSM nozzles were calculated and imposed at the nozzle inlet boundary as shown in Fig. 7. The non-dimensional conservative flow quantities at the nozzle inlet boundary were calculated given the nozzle total inlet conditions (P_0, T_0, γ, MW), the throat to inlet area ratio (A_t/A_i) and the free-stream conditions (M_∞, P_∞, T_∞, ρ_∞, $\bar{q}$). The inlet boundary values were calculated using one-dimensional isentropic relations for a sonic throat. The boundary conditions were applied as uniform constant values at the inlet face.

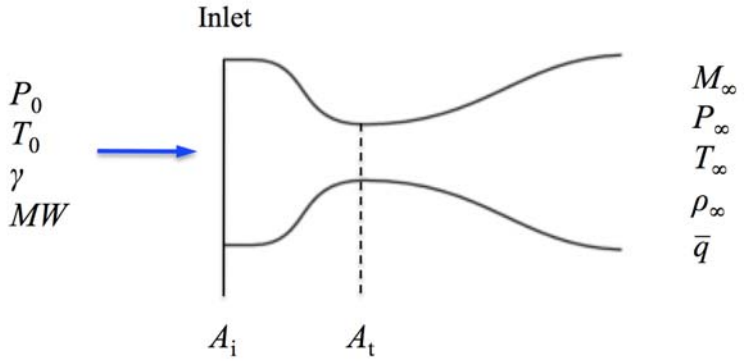

Figure 7. BSM nozzle inputs schematic.

V. CFD Model Validation

In order to ascertain if pressure on the LO2 portion of the tank is accurately predicted with the use of the simplified model without the BSMs, the ET+SRBs and the full fidelity ET-128 DCR solutions were compared. Two steady-state solutions were computed at flight conditions for a mission-elapsed time of 123 seconds. The simplified ET+SRBs solution was run 4,000 steady-state steps plus an additional 1,000 pseudo time-accurate steps with dual-time sub-iterations to improve convergence. The constant CFL number time scaling option based on local cell Reynolds number was employed. The ET-128 DCR solution utilized a similar strategy with 6,500 steady-state and 1,500 time-accurate steps.

Figure 8 illustrates the geometry and coordinates of the ET, where the angle ϕ is defined to be 0 degrees at the +Z in the Y_T=0 plane with counter-clockwise rotation about the +x axis considered positive. The comparison of the two models was made by plotting constant ϕ-cuts of pressure on the LO2 ET surface at ϕ=0, 10, 20, 31.5, 40, 50 and 60 degrees as shown in Figure 9. The difference in pressure (ΔP) between the two different CFD flow fields was computed. Figure 10 shows contours of the computed pressure in psia on the surface of both CFD solutions, and in the center are shown color contours of ΔP. In the center image, the gray represents zero difference; red represents higher pressure in the simplified geometry, and blue denotes lower pressure.

As evidenced by the line- and ΔP-plots, good agreement exists between the solutions, with differences attributed only due to missing IFRs, pressurization lines, protuberances and the Orbiter (not shown). Mach number contours extracted at the Y_T=0 plane are shown in Fig. 11. Both the ET-128 DCR and the simplified ET+SRBs models exhibited similar shock structures forward of the intertank. Modeling the Orbiter and detailed protuberances was not necessary to accurately predict the pressure on the LO2 ET, apart from the local differences caused by the protuberances.

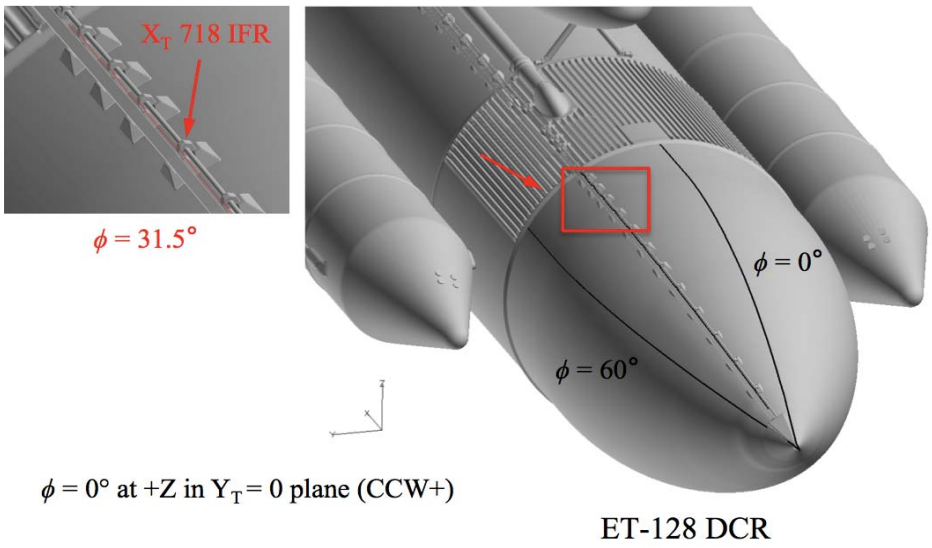

Figure 8. Definition of the angle ϕ on LO2 ET surface.

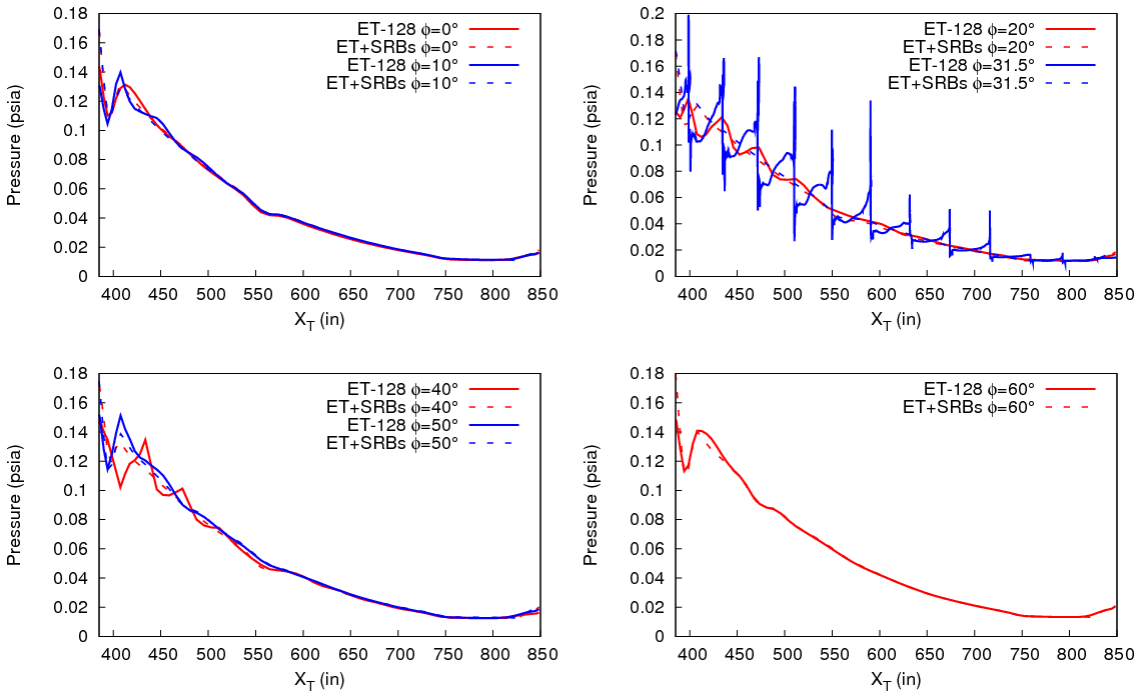

Figure 9. ET-128 DCR versus ET+SRBs without BSMs ϕ-cuts of pressure on LO2 ET surface at MET=123 sec, Mach=3.909, α=4.3°, β=0.081°.

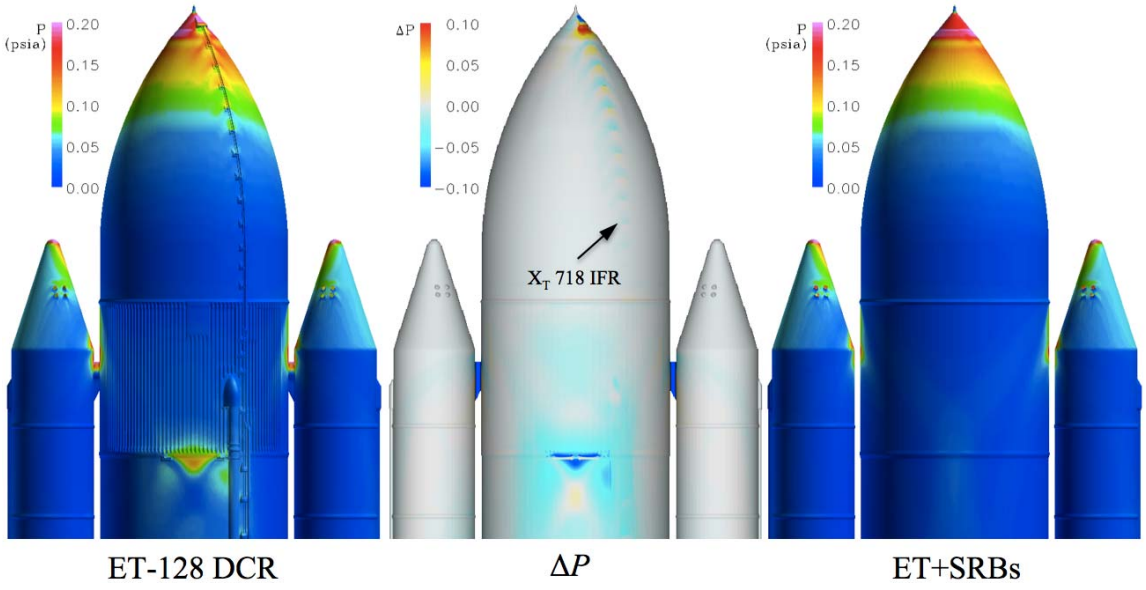

Figure 10. ET-128 DCR versus ET+SRBs without BSMs ΔP at MET=123 sec, Mach=3.909, α=4.3°, β=0.081°.

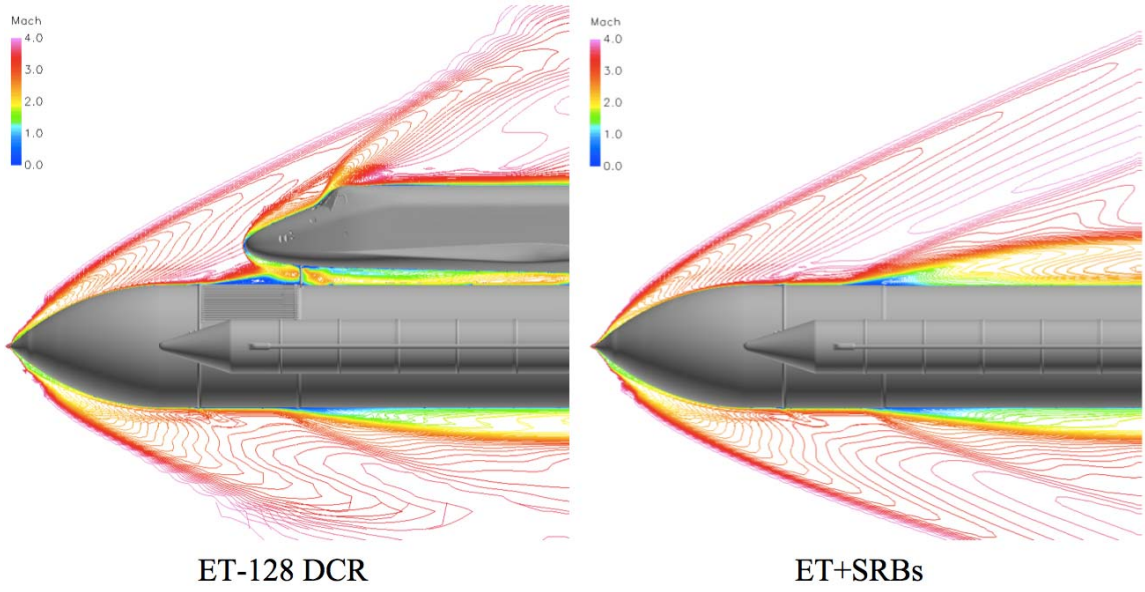

Figure 11. ET-128 DCR versus ET+SRBs without BSMs Mach number contours at MET=123 sec, Mach=3.909, α=4.3°, β=0.081°.

VI. Pressure Extraction

During the firing of the BSMs, pressure (P) was extracted from a point located at (X_T, Y_T, Z_T, ϕ)=(718.0, 86.4, 540.99, 31.5). This point coincides with the location of the X_T 718 LO2 IFR in the ET-128 DCR geometry. Calculated at each time step, the maximum pressure (P_{max}) and the maximum difference in pressure (ΔP_{max}) occurring at this location were also computed from a grid-subset depicted in Fig. 12. The grid-subset was comprised of a series of points located on the ET surface (L=1) and provided a better measure of the pressure bounds. The P_{max} corresponds to the maximum value of all the points in the grid sub-set. The ΔP_{max} value was computed using:

$$\Delta P_{max} = P_{max\ BSMs\ firing} - P_{max\ BSMs\ cold} \tag{1}$$

where $P_{max\ BSMs\ firing}$ represents the P_{max} from the time-accurate simulation and $P_{max\ BSMs\ cold}$ is P_{max} from the steady-state solution.

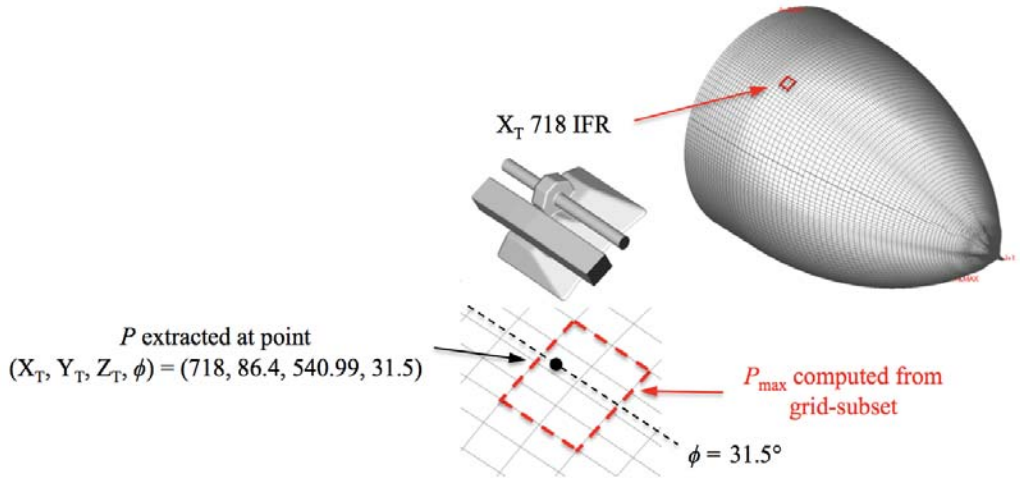

Figure 12. Pressure extraction on ET surface from a point and from a grid-subset.

VII. BSM Nozzles Thrust Calibration

The simplified ET+SRBs+BSMs model was used to calibrate the thrust of the nozzles. The calibration was performed by running multiple cases each with a different value of the nozzle inlet total pressure (P_0), computing the thrust from each of the CFD solutions and selecting the value of P_0 which matched the known thrust. The calibration cases were run at MET=123 second flight conditions with Mach=3.909 and α=4.3°. The nozzle inlet conditions (P_0, T_0, γ, MW) obtained from a NASA Glenn Research Center proprietary report were utilized (see Table 2). Since the range of the data was limited to $600 \le P_0 \le 1000$, 1-D linear extrapolation was used to find values for T_0 and MW at P_0=1200, 1400, 1600, 1700, 1800 and 2000 psia. A total of 11 quasi steady-state solutions were computed with the BSMs firing on the Columbia supercomputer using 128 CPUs. The solutions were run 4,000 steady-state steps with BSMs cold (turned off), and restarted with BSMs firing for an additional 1,000 pseudo time-accurate steps. To achieve better convergence, five dual-time sub-iterations were utilized.

The thrust of the BSMs was integrated from the momentum flux across each nozzle exit face using the MIXSUR and OVERINT[25] codes. The calculated thrust and naming convention of the BSM motors are shown in Table 2 and Fig. 13. A plot of the thrust as a function of P_0 is presented in Fig. 14. As expected, the calibration runs showed that the thrust produced by each BSM is approximately equivalent and increases linearly with P_0.

According to Ref. 26 the BSM motors provide an average thrust of 18,500 lbs each and have a total minimum impulse of 15,000 Lb-sec. Using the nozzle inlet total pressure of P_0=1700 psia, the integrated thrust from the CFD solution was matched within 142 lbs or 0.8% of the average value. As a result, the nozzles inlet conditions (P_0=1700 psia, T_0=6267.6 deg, γ=1.22, MW=28.697 g/mol) were selected from the calibration cases for the steady-state plume and time-accurate BSM IOP simulations.

Table 2. BSM nozzles inlet conditions and integrated thrust.

P_0 psia	T_0 R	γ	MW g/mol	*Thrust* (lbf)							
				bsm1l	bsm2l	bsm3l	bsm4l	bsm1r	bsm2r	bsm3r	bsm4r
600.0	6091.2	1.22	28.363	6,581.0	6,581.2	6,581.0	6,581.0	6,581.0	6,581.3	6,581.0	6,581.0
700.0	6114.6	1.22	28.405	7,678.8	7,679.2	7,678.9	7,678.9	7,678.8	7,679.2	7,678.9	7,678.9
800.0	6134.4	1.22	28.441	8,776.9	8,777.2	8,776.9	8,776.9	8,776.9	8,777.3	8,776.9	8,777.0
900.0	6152.4	1.22	28.473	9,874.9	9,875.3	9,874.9	9,874.9	9,874.8	9,875.4	9,874.8	9,875.0
1000.0	6166.8	1.22	28.501	10,971.3	10,971.8	10,971.5	10,971.4	10,971.3	10,971.9	10,971.3	10,971.4
1200.0	6195.6	1.22	28.557	13,160.7	13,160.9	13,160.1	13,160.7	13,160.5	13,161.2	13,160.5	13,160.7
1400.0	6224.4	1.22	28.613	15,352.8	15,353.4	15,352.9	15,352.6	15,352.2	15,353.7	15,352.4	15,352.9
1600.0	6253.2	1.22	28.669	17,545.6	17,545.3	17,545.3	17,545.1	17,545.1	17,546.1	17,545.3	17,545.7
1700.0	6267.6	1.22	28.697	18,641.7	18,641.6	18,641.4	18,641.6	18,640.9	18,642.1	18,641.3	18,641.3
1800.0	6282.0	1.22	28.725	19,736.6	19,738.2	19,738.2	19,737.8	19,738.0	19,738.7	19,737.5	19,738.1
2000.0	6310.8	1.22	28.781	21,930.8	21,931.5	21,930.0	21,930.5	21,930.4	21,931.2	21,930.7	21,930.7

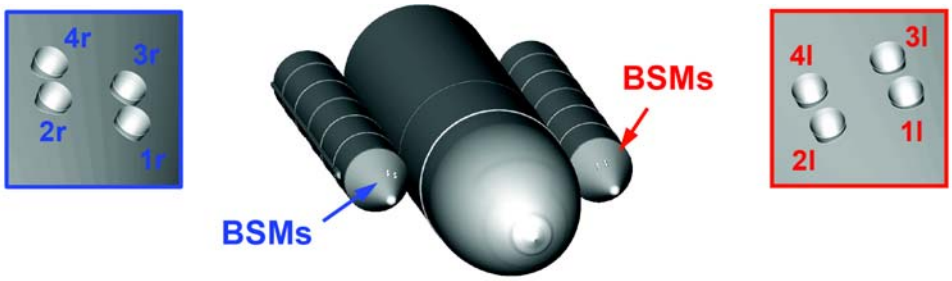

Figure 13. BSM nozzles naming convention.

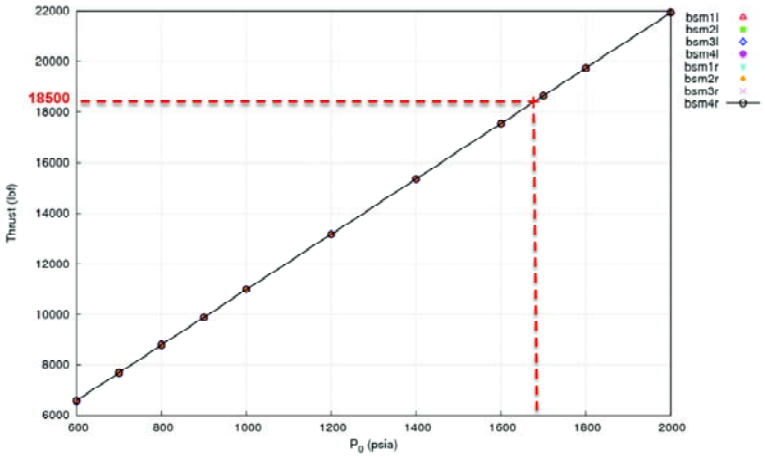

Figure 14. BSM nozzles thrust versus nozzle inlet total pressure from the thrust calibration cases.

VIII. BSM IOP Simulations

The simplified ET+SRBs+BSMs model was used to perform time-accurate IOP simulations with a very small time step. A converged steady-state solution with the BSMs cold (turned off), was restarted in time-accurate mode with the BSMs firing (power BCs turned on). The nozzle inlet conditions selected from the BSM thrust calibration were employed. The total simulation time in the computations was on the order of 0.01 seconds. The motion of the SRBs relative to the rest of the vehicle is neglected, which is a reasonable approximation during this short time interval.

The Newton and dual-time stepping algorithms with sub-iterations were employed in OVERFLOW. When using the Newton time-stepping option (*ITIME*=0), the computational time-step remains constant and no time-step scaling is applied. The dual-time stepping method is an implicit numerical method for time-accurate integration of the numerical equations in which a pseudo-time iteration is embedded into each physical-time step (see Rogers et al.[27]). The dual-time stepping advances the solution one physical time-step at the end of each sub-iteration cycle and allows use of relatively large physical-time steps compared to the Newton method.

The key parameters involved in the unsteady IOP runs included *DT* (inner-iteration time-step size), *DTPHYS* (outer-iteration time-step size), the number of Newton/dual sub-iterations (*NITNWT*) and the time-step scaling option (*ITIME*). In theory, when running with dual-time stepping, *DTPHYS* is set based on physics of the problem and *DT* is set based on the numerical requirements of the solution. Moreover, *DTPHYS* provides the desired time resolution, whereas *DT*, *ITIME* and *CFL* number facilitate the stability and convergence of the inner iterations.

Parametric studies were utilized to find optimal choices of *DT*, *DTPHYS*, *NITNWT* and *ITIME* to yield the best converged solution. The following parameters were used:

- *DT*=0.0; *ITIME*=0 for Newton time stepping
- *DT*=0.01, 0.001; *ITIME*=1 for dual-time stepping
- *DTPHYS*=1.0, 0.5, 0.25, 0.125
- *NITNWT*=10, 20, 40, (80, 160 for *DTPHYS*=0.125)

In OVERFLOW the variable *DT* is non-dimensionalized by the free-stream speed of sound, while *DTPHYS* is non-dimensionalized by the reference velocity (U_{ref}). The dimensional physical time step (Δt) in seconds is given by:

$$\Delta t = \frac{DTPHYS \quad L_{ref}}{U_{ref}} \tag{2}$$

where reference length L_{ref} =1 inch and U_{ref} =4204.39 ft/sec, which is the local speed of sound for the Mach=3.909 cases.

The computations were run on the Harpertown nodes of the Pleiades supercomputer using 256 and 512 cores. Each of these nodes contains Intel 3GHz Xeon E5472 dual quad-core processors with 8GB of memory and 1GB per

core. Pleiades is a distributed-memory SGI ICE cluster connected with InfiniBand in a dual-plane hypercube topology. The time-accurate IOP simulations required 5,000 steady-state plus an additional 1,000 to 16,000 time-accurate steps. Due to numerical instability issues, these solution can be difficult to compute resulting in negative density or pressure.

IX. CFD Solution and Convergence

Although the CFD simulations exhibited varying levels of convergence, a number of solution trends could be inferred. In general, the speed of the over-pressure wave increased with a greater number of *NITNWT* sub-iterations and smaller physical time step *DTPHYS*. A plot of the pressure at a point on the X_T 718 ice/frost ramp plotted versus time is shown in Figs. 15 and 16. An increase in the wave speed can be seen in Fig. 15, where *DTPHYS* is progressively reduced by a factor of two, from 1.0 to 0.125, while *NITNWT*=40 is held constant. For some of the cases the amplitude of the wave was similar, but occurred at a different frequency as shown in Fig. 16, where the value of *DTPHYS* is fixed at 0.125 and *NITNWT* increases from 10 to 160.

In the time-accurate IOP simulations, using a smaller physical time-step and larger number of sub-iterations yielded better convergence, but significantly increased the computational cost. Cases that employed *DTPHYS*>0.5 were unable to adequately resolve the time-domain with Δt being too large. Using fewer than 40 sub-iterations was insufficient and yielded only marginal convergence.

The results of the parametric studies were deemed adequate to capture the maximum pressure peak of the initial wave. The best IOP solution was achieved with the case: 1) *DTPHYS*=0.125, *DT*=0.0, *NITNWT*=40 and *ITIME*=0. The solution convergence plots from this case are shown in Fig. 17 and 18. Comparable results were attained with the case: 2) *DTPHYS*=0.125, *DT*=0.001, *NITNWT*=160 and *ITIME*=1. These two cases yielded similar results, but case 1 used 20% of CPU time of case 2.

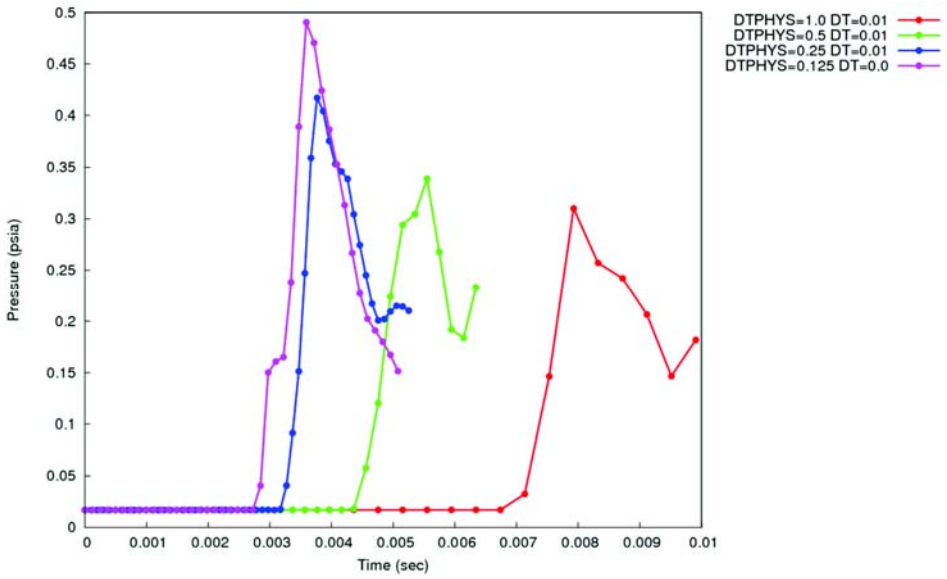

Figure 15. Pressure versus time on the ice/frost ramp at (X_T, Y_T, Z_T, ϕ)=(718.0, 86.4, 540.99, 31.5) for *NITNWT*=40 sub-iterations.

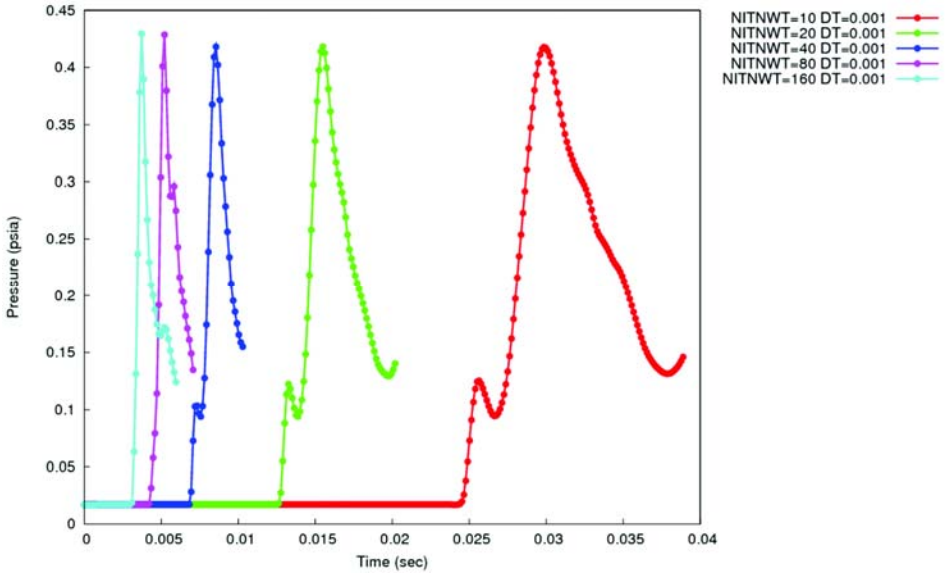

Figure 16. Pressure versus time on the ice/frost ramp at (X_T, Y_T, Z_T, ϕ)=(718.0, 86.4, 540.99, 31.5) for *DTPHYS*=0.125.

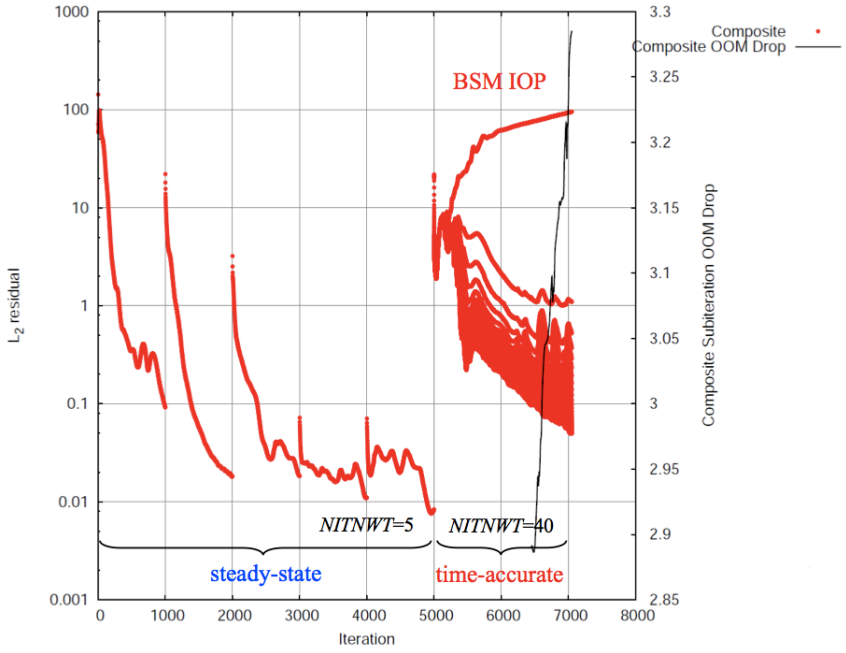

Figure 17. L2 norm of OVERFLOW normalized residual for *DTPHYS*=0.125, *DT*=0.0, *NITNWT*=40 and *ITIME*=0.

The L2 norm of the normalized residual fore case 1 is plotted in Fig. 17. The plot shows the convergence of the residual during the coarse-grid sequencing used during the first 2000 time steps, as well as the dual-time stepping used between the time steps of 4000 and 5000. The BSM firing simulation begins during time-step number 5001 at which time case 1 used 40 sub-iterations per time step. After the next several hundred time steps it can be seen that the residual is converging fairly well at each time step, but prior to this even 40 sub-iterations was probably not adequate to compute the initial firing.

X. Results

In order to quantify the effects of the BSMs firing, differences in pressure were examined between CFD solutions with and without the motors. The computed pressure on the surface of the vehicle, and the difference between the BSMs cold and steady-state plume solution of the BSMs firing is shown in Fig. 18. At the ET IFR X_T 718 point location computing the ΔP yielded 0.12 psid.

The results of the time-accurate BSM IOP parametric studies produced plots of the over-pressure pulse as a function of time. Plots of P and P_{max} versus time (in seconds) extracted at a point and from the IFR grid-subset are shown in Figures 19 and 20 respectively. The values of the dimensional simulation time step (ΔT), flow solver iteration (*NSTEPS*) and time at which ΔP_{max} occurred $T(\Delta P_{max})$ are included in Table 3. The maximum pressure peak was found between T=0.00347 and 0.03035 seconds and ranged from 0.2607 to 0.7929 psia.

Using the best converged case (*DTPHYS*=0.125, *DT*=0.0, *NITNWT*=40 and *ITIME*=0), the values of P_{max}=0.6239 psia, ΔP_{max}=0.605 psid were obtained at T=0.00347 seconds. The computed pressure on the surface of the ET+SRBs, and ΔP between BSMs cold and BSMs firing solutions is shown in Fig. 21. The flow visualization of the BSM IOP and plume impingement (at P_{max} condition) is presented in Fig. 22. This figure plots the species mass fraction of the BSM gas using a cutting plane at X_T=827 inches. In addition to the grid-subset (IFR location), pressure contours are displayed on the surface of the ET+SRBs.

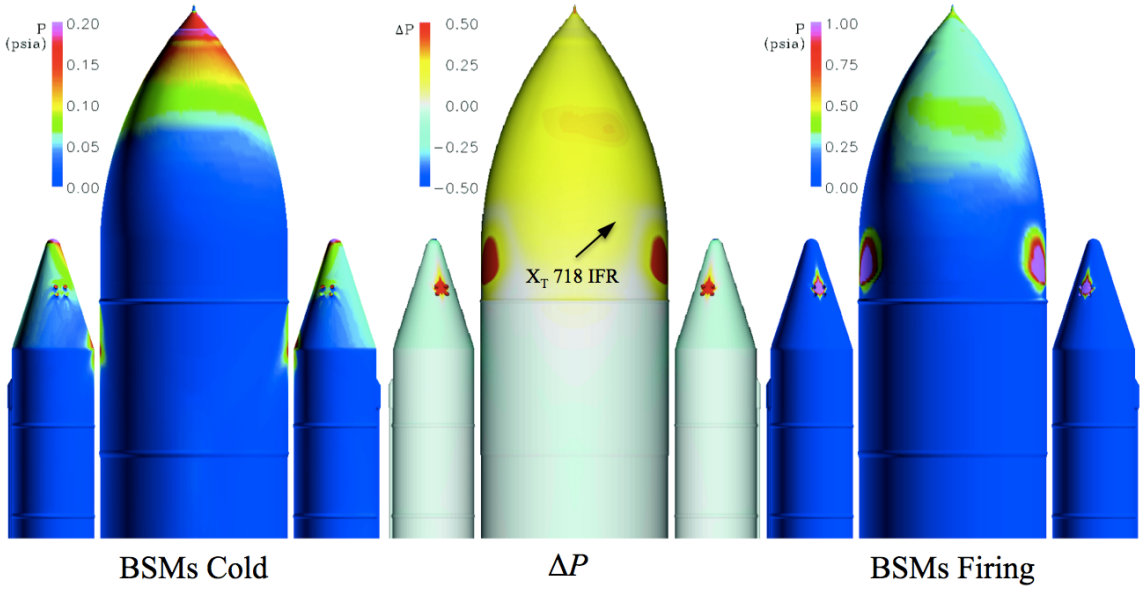

Figure 18. ET+SRBs+BSMs steady-state solution ΔP at MET=123 sec, Mach=3.909, α=4.3°, β=0.081°.

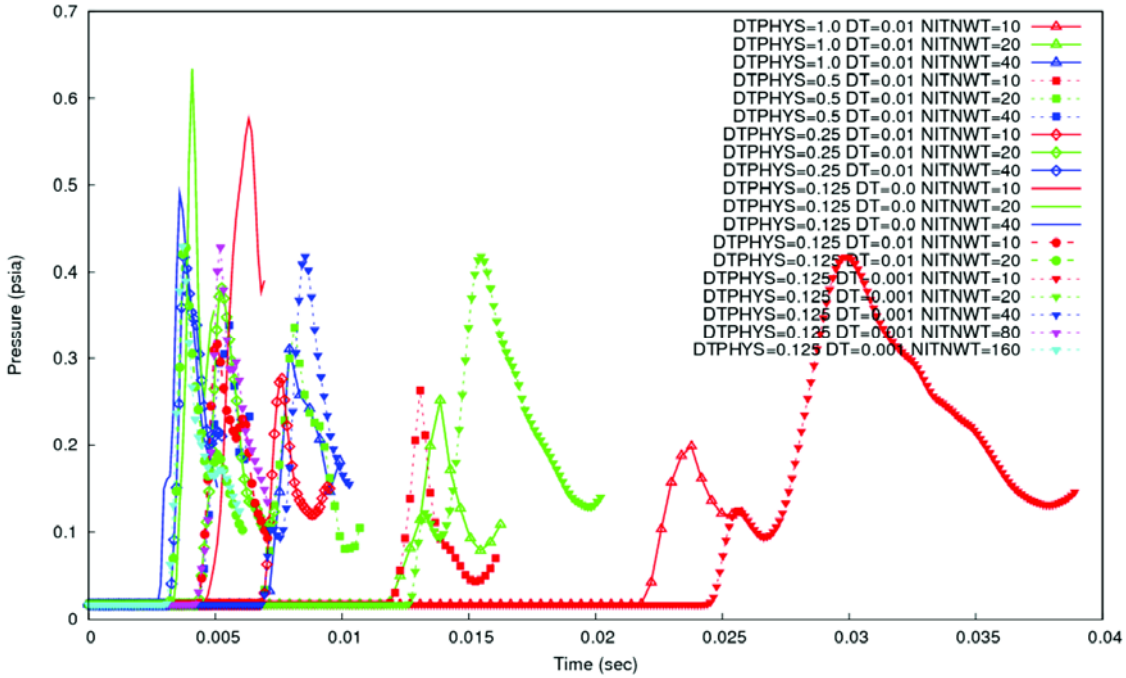

Figure 19. Pressure versus time on the ice/frost ramp at (X_T, Y_T, Z_T, ϕ)=(718.0, 86.4, 540.99, 31.5).

6

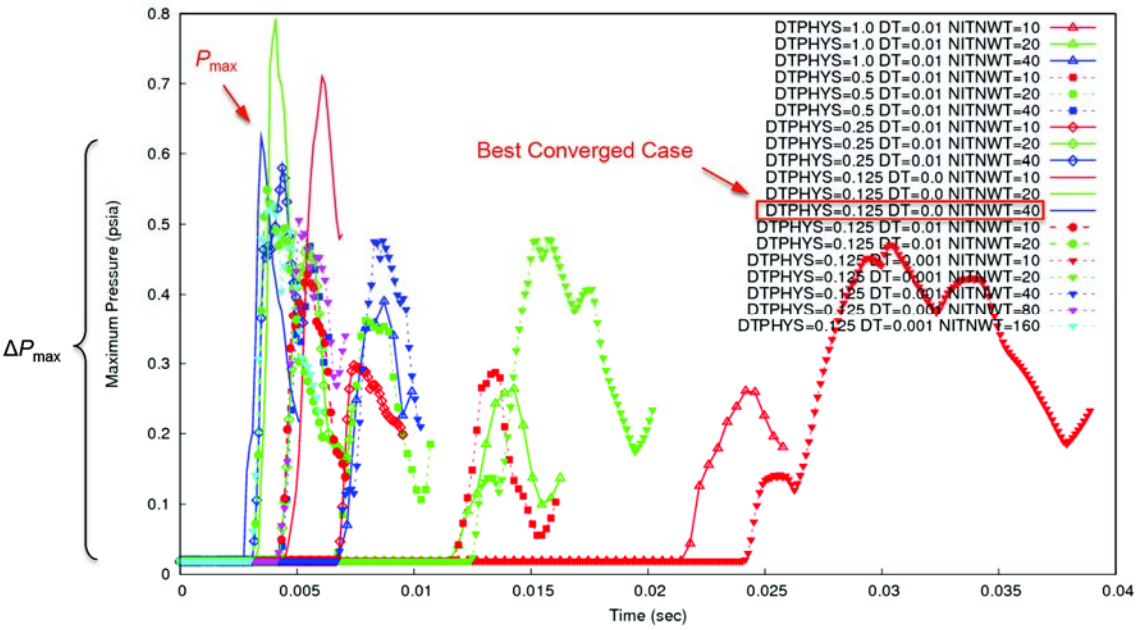

Figure 20. Maximum pressure versus time on the ice/frost ramp from a grid-subset.

Table 3. Results of the parameter study showing P_{max} and ΔP_{max} from ET X_T IFR grid-subset.

NITNWT	DTPHYS	DT	ITIME	ΔT sec	T (ΔPmax) sec	Pmax psia	ΔPmax psid	NSTEPS	NCPUs	CPU Time Hrs	Wallclock Time Hrs
10	1.0	0.01	1	1.982E-05	0.02418	0.2607	0.2418	6540	256/512	9,053.0	39.84
20	1.0	0.01	1	1.982E-05	0.01427	0.2638	0.2449	6000	256	11,321.9	53.34
40	1.0	0.01	1	1.982E-05	0.00872	0.3902	0.3713	6000	256	20,978.4	91.20
10	0.5	0.01	1	9.910E-06	0.01348	0.2874	0.2685	7060	256/512	11,309.0	46.48
20	0.5	0.01	1	9.910E-06	0.00793	0.3614	0.3425	7020	256	22,214.8	98.39
40	0.5	0.01	1	9.910E-06	0.00555	0.4684	0.4495	6020	256	20,709.3	90.35
10	0.25	0.01	1	4.955E-06	0.00743	0.2973	0.2784	9010	256	24,041.7	111.42
20	0.25	0.01	1	4.955E-06	0.00545	0.4664	0.4475	7020	256	20,868.5	93.22
40	0.25	0.01	1	4.955E-06	0.00436	0.5804	0.5615	7020	256	40,229.5	169.14
10	0.125	0.0	0	2.478E-06	0.00607	0.7102	0.6913	7850	512	14,735.4	39.92
20	0.125	0.0	0	2.478E-06	0.00409	0.7929	0.7740	7450	512	24,136.3	57.65
40	0.125	0.0	0	2.478E-06	0.00347	0.6239	0.6050	7050	512	39,607.7	88.46
10	0.125	0.01	1	2.478E-06	0.00545	0.4291	0.4102	7850	512	15,146.1	43.66
20	0.125	0.01	1	2.478E-06	0.00372	0.5492	0.5303	7450	512	24,744.8	61.17
10	0.125	0.001	1	2.478E-06	0.03035	0.4711	0.4522	21150	512	82,138.6	182.22
20	0.125	0.001	1	2.478E-06	0.01573	0.4785	0.4596	13150	512	80,964.2	173.88
40	0.125	0.001	1	2.478E-06	0.00867	0.4768	0.4579	9150	512	80,461.2	169.36
80	0.125	0.001	1	2.478E-06	0.00508	0.5059	0.4870	7850	512	110,904.9	229.48
160	0.125	0.001	1	2.478E-06	0.00396	0.5278	0.5089	7400	512	182,627.9	355.01

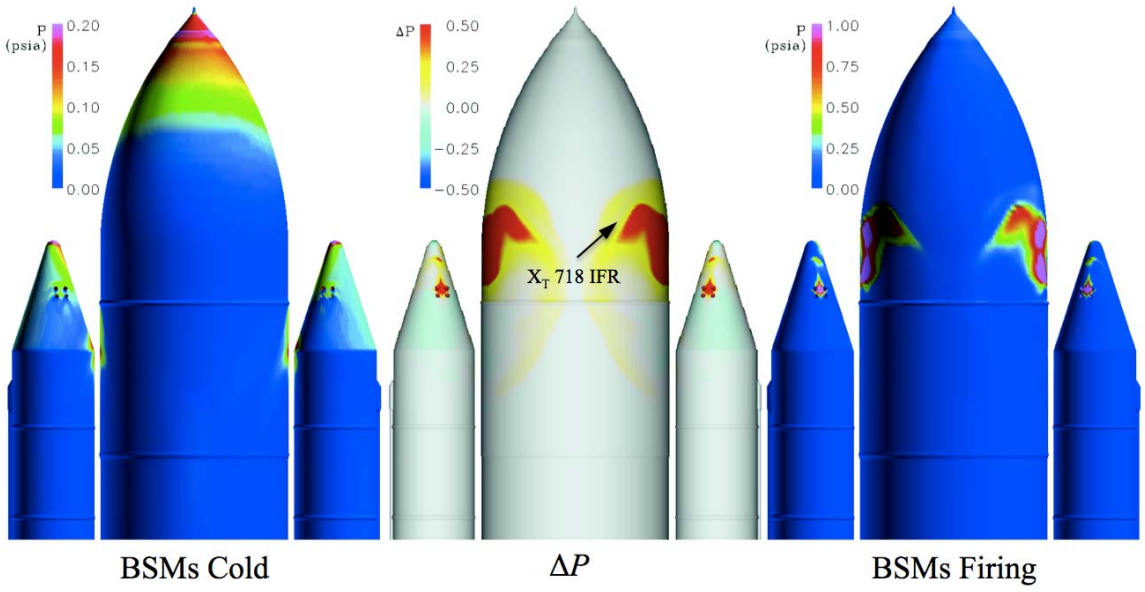

Figure 21. ET+SRBs+BSMs time-accurate solution ΔP at MET=123 sec, Mach=3.909, α=4.3°, β=0.081°.

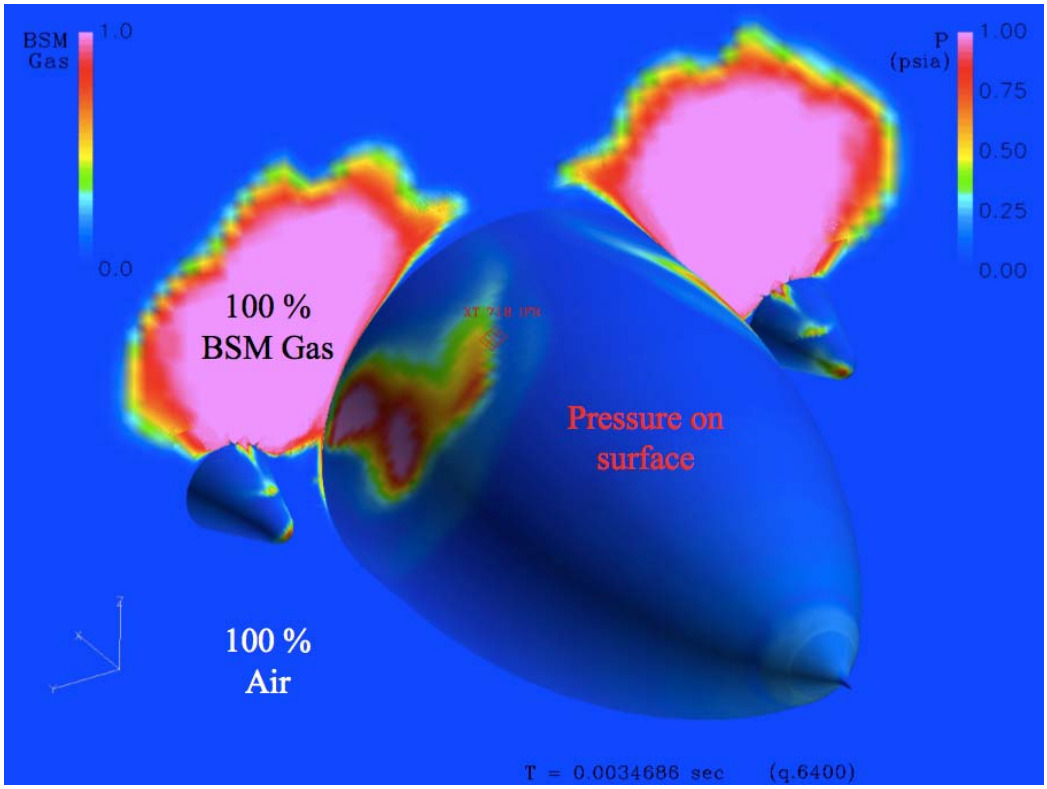

Figure 22. Species mass fraction of BSM gas cutting plane at X_T=827 inches and pressure on the surface for *DTPHYS*=0.125, *DT*=0.0, *NITNWT*=40 and *ITIME*=0 case at MET=123 sec, Mach=3.909, α=4.3°, β=0.081°.

XI. Data Comparisons

A steady-state OVERFLOW simulations of the SRB separation with both forward and aft BSMs; and forward RCS jets firing were performed by the Boeing Co. in 2003. Using the SSLV with high geometric fidelity, five quasi steady-state, Mach 4.0 cases were computed at 0.0, 0.7, 0.75, 1.0 and 1.5 seconds after the SRB separation command. The relative position of the SRBs was derived from Monte Carlo analysis. The BSM thrust levels of 100%, 52%, 13% and 3% were employed. The RCS thrusters were turned on except in the 3% BSM thrust level case. A variable γ approach with three different gas species (Air, RCS gas, BSM gas) was used in OVERFLOW. These steady-state BSM and RCS plume simulations did not model the over-pressure phenomenon. A pressure increase of 0.2 psid on the ET surface was reported in this work and was considered negligible compared to the design pressures. The steady-state plume solutions of the forward BSMs firing from the present study yielded a lower ΔP value of 0.12 psid at the IFR location. In comparison, the time-accurate IOP simulations of the BSMs firing produced a ΔP_{max} of 0.61 psid.

A ground-firing test of a single BSM was performed at Marshal Space Flight Center in an effort to quantify the IOP pulse at various locations in the far field. Instrumentation measured the pulse at locations of 40 feet, 94.5 feet, and 120 feet from the BSM nozzle exit, and at angular orientations of 0, 30, and 45 degrees from the centerline of the BSM nozzle. On the actual flight vehicle, the X_T=718 IFR is 17.6 feet from the right-hand forward BSM cluster and at a 27 degree angular orientation. The ground-firing pressure data exhibited a decay inversely proportional to the distance from the motor, indicating a two-dimensional behavior. Using this decay rate and extrapolating, the 30-degree ground-test pressure pulse at a distance of 17.6 feet would be approximately 1.0 psid. The investigators noted that this two-dimensional behavior is probably due to the effect of the ground, and that in flight, the decay would likely be inversely proportional to the square of the distance, and thus should be less than 1.0 psid. To account for the fact that the flight hardware uses a cluster of four BSMs, a factor of 1.4 increase in the pressure pulse was proposed by the investigators. Finally, they note that the difference in altitude between the ground test and the flight vehicle during BSM firing should result in a further drop in the IOP pulse on the flight vehicle. In summary, they

concluded that the BSM IOP is conservatively bounded by 1.4 psid. Thus the current result of approximately 0.6 psid is consistent with these previous estimates.

XII. Computing Resources

This section provides resource metrics from the use of the Columbia and Pleiades supercomputers. A total of 11 quasi steady-state BSM thrust calibration cases were run on Columbia using 64 and 128 CPUs. Each case required 5,000 to 8,000 time-steps to compute the passage of the IOP beyond the IFRs. Each case used 2,500 to 8,200 CPU hours, and 39 to 58 hours of wall-clock time. A total of 51,800 CPU hours were spent running these cases.

Table 3 includes a summary of the computational resources to run 19 time-accurate BSM IOP cases on Pleiades using 256 and 512 processors. Each case required 6,000 to 21,500 steps to converge, used 9,000 to 182,700 CPU hours, and 40 to 355 hours of wall-clock time. A total of 836,200 CPU hours were consumed running these cases. The computational grids of the simplified SSLV model contained 50.1 million grid points and 46 zones. A typical time-accurate OVERFLOW run created 100 3.4GB solution files and required over 350GB of disk space storage.

XIII. Conclusions

An assessment of the BSM IOP was performed on the space shuttle ET X_T 718 ice-frost ramp at MET of 123 seconds using the OVERFLOW code on the Columbia and Pleiades supercomputers. A simplified model of the SSLV consisting of a truncated ET+SRBs geometry with forward BSM nozzle+plume grids was developed to model the Mach 4.0 flow field. The simplified model was validated by comparisons to high fidelity SSLV (ET-128 DCR) solutions. The thrust of the BSM nozzles was integrated and calibrated to match the known thrust of the motors. Time-accurate parametric studies were conducted to find the best converged and most accurate solution. The current study identified key flow solver parameters to attain an acceptable level of solution accuracy and space-time convergence. The effects of the over-pressure and ΔP were calculated on the surface of the tank at the IFR location.

The steady-state plume solutions of the simplified ET+SRBs model produced a ΔP of 0.12 psid at the X_T 718 IFR location. The time-accurate BSM IOP simulations yielded a maximum pressure of 0.62 psia and maximum delta pressure of 0.61 psid occurring at 0.004 seconds after motor ignition. The results of this study were compared to previous steady-state OVERFLOW solutions of the SRB separation with BSMs and RCS jets firing. These BSM/RCS steady-state plume computations yielded a higher ΔP of 0.2 psid on the ET surface. The results from the present work are lower than BSM IOP ground test data ΔP_{max} of 1.4 psid. The predicted IOP loads on the X_T 718 IFR were well below the design limit of 8.4 psid. Thus it can be concluded that the firing of the BSM was not a contributing factor to the loss of foam from the LO2 IFR.

Acknowledgments

The authors would like to acknowledge Dr. Jasim Ahmad and Dr. William Chan for their invaluable help, and the staff at NASA Advanced Supercomputing (NAS) facility at Ames Research Center for providing computing resources and user support.

References

[1]Dismukes, K., "SRB Overview," NASA Human Space Flight, April 2002,
URL: http://spaceflight.nasa.gov/shuttle/reference/shutref/srb/srb.html [cited 10 February 2011].

[2]Smith, G. W., and Chase, C. A., "Space Shuttle Booster Separation Motor Design," AIAA Paper 1976- 772, *American Institute of Aeronautics and Astronautics and Society of Automotive Engineers 12th Propulsion Conference*, Palo Alto, Calif., July 26-29, 1976.

[3]Elchert, K. C., "Space Shuttle Solid Rocket Booster Separation System," AIAA Paper 1982-1556, Guidance and Control Conference, San Diego, CA, August 9-11, 1982.

[4]Chase, C. A., Fisher, K. M., and Eoff, W., "The Qualification of the Shuttle Booster Separation Motors," AIAA Paper 1978-983, *American Institute of Aeronautics and Astronautics and Society of Automotive Engineers 14th Joint Propulsion Conference*, Las Vegas, NV, July 25-27, 1978.

[5]Colombier R., and Pollet M., "Solid Rocket Motor Ignition Overpressure Prediction," AIAA Paper 1991-2437, *27th Joint Propulsion Conference*, Sacramento, CA, June 24-26, 1991.

[6]Housman, J. A., Barad, M. F., Kiris C., "Space-Time Accuracy Assessment of CFD Simulations for the Launch Environment," AIAA Paper 2011-3650, 29th AIAA Applied Aerodynamics Conference, Honolulu, HI, June 2011.

[7]Gea, L. M., and Vicker, D., "CFD Simulation of the Space Shuttle Launch Vehicle with Booster Separation Motor and Reaction Control System Plumes," *Proceedings of the Third International Conference on Computational Fluid Dynamics*, ICCFD3, Toronto, July 12-16, 2004.

[8]Jespersen, D. C., Pulliam, T. H., and Buning, P. G., Recent Enhancements to OVERFLOW, AIAA Paper 97-0644, Jan. 1997.
[9]Buning, P. G., Jespersen, D. C., Pulliam, T. H., Klopfer, G. H., Chan, W. M., Slotnick, J. P., Krist, S. E., and Renze, K. J., Overflow Users Manual, Version 1.8aa NASA Langley Research Center, Hampton, VA, 2003.
[10]Slotnick, J. P., Buning, P. G., Kandula, M., and Martin, F. W., Jr., "Numerical Simulation of the Space Shuttle Launch Vehicle Flowfield with Real Gas Solid Rocket Plume Effects," AIAA Paper 93-0521, AIAA 31st Aerospace Sciences Meeting, Reno, NV, Jan. 1993.
[11]Kandula, M., Pearce, D. G., Labbe, S. G., and Martin, F. W., Jr., "Effect of Solid Rocket Exhaust Plume on Space Shuttle Orbiter Flowfield," 19th JANNAF Exhaust Plume Technology Subcommittee Meeting, U.S. Army Missile Command, Redstone Arsenal, AL, May 1991.
[12]Chan, W. M., Developments in Strategies and Software Tools for Overset Structured Grid Generation and Connectivity, AIAA Paper 2011-3051, 20th AIAA Computational Fluid Dynamics Conference, Honolulu, HI, June, 2011.
[13]Chan, W. M., "The Overgrid Interface for Computational Simulations on Overset Grids," AIAA Paper 2002-3188, Jun. 2002.
[14]Chan, W. M., and Buning, P. G., "Surface Grid Generation Methods for Overset Grids," Computers & Fluids, Vol. 24, No. 5, 1995, pp. 509-522.
[15]Chan, W. M., Gomez, R. J., Rogers, S. E. and Buning, P. G., "Best Practices in Overset Grid Generation," AIAA Paper 2002-3191, *32nd AIAA Fluid Dynamics Conference*, St. Louis, Missouri, Jun. 2002.
[16]Rogers, S. E., Suhs, N. E., and Dietz, W. E., "PEGASUS 5: An Automated Pre-processor for Overset- Grid CFD," AIAA Journal, Vol. 41, No. 6, June, 2003, pp. 1037-1045.
[17]Chan, W. M., "Enhancements to the Hybrid Mesh Approach to Surface Loads Integration on Overset Structured Grids," AIAA Paper 2009-3990, 19th AIAA Computational Fluid Dynamics, San Antonio, TX, June 22-25, 2009.
[18]Biswas, R., Djomehri, M. J., Hood, R., Jin, H., Kiris, C., and Saini, S., "An Application-Based Performance Characterization of the Columbia Supercluster," Supercomputing Conference, Seattle, WA, 2005.
[19]Biswas, R., "Impact of the Columbia Supercomputer on NASA Space and Exploration Missions," *Proceedings of 2nd IEEE International Conference on Space Mission Challenges for Information Technology*, Pasadena, CA, July, 2006.
[20]Pulliam, T. H., and Jespersen, D. C., "Large Scale Aerodynamic Calculation on Pleiades," *Proceedings of the 21st International Conference on Parallel Computational Fluids Dynamics*, Moffett Field, CA, May 18-22, 2009.
[21]Benek, J. A., Buning, P. G., and Steger, J. L., "A 3-D CHIMERA Grid Embedding Technique," AIAA- 85-1523-CP, Jul. 1985.
[22]Tramel, W. R., Nichols, R., and Buning, P. G., "Addition of Improved Shock-Capturing Schemes to OVERFLOW 2.1," AIAA Paper 2009-3988, 19th AIAA Computational Fluid Dynamics, San Antonio, Texas, June 22-25, 2009.
[23]Nichols, R., and Buning, P. G., "Solver and Turbulence Model Upgrades to OVERFLOW 2 for Unsteady and High-Speed Applications," AIAA Paper 2006-2824, *24th AIAA Applied Aerodynamics Conference*, San Francisco, California, June 5-8, 2006.
[24]Spalart, P. R., and Allmaras, S. R., "A One-Equation Turbulence Model for Aerodynamic Flows," AIAA Paper 92-0439, Jan. 1992.
[25]Chan, W. M. and Buning, P. G., "User's Manual for FOMOCO Utilities - Force and Moment Computation Tools for Overset Grids," NASA TM 110408, July 1996.
[26]General Dynamics Corp., "Liquid Rocket Booster Study Final Report," Vol. 2, NASA-CR-183600, March 1989.
[27]Rogers, S. E., Kwak, D., and Kiris, C., "Numerical Solution of the Incompressible Navier-Stokes Equations for Steady-State and Time-Dependent Problems," AIAA Paper 89-0463, Jan. 1989.
[28]Kao, D. L., and Chan, W. M., "OVERSMART - A Solution Monitoring and Reporting Tool for the OVERFLOW Flow Solver," AIAA Paper 2009-3998, *19th AIAA Computational Fluid Dynamics Conference*, San Antonio, Texas, Jun. 2009.